MICROSCALE LASER PEEN FORMING OF SINGLE CRYSTAL: DYNAMIC DEFORMATION AND ANISOTROPY

Yajun Fan, Youneng Wang, Jeffrey W. Kysar, and Y. Lawrence Yao
Department of Mechanical Engineering
Columbia University
New York, New York

KEYWORDS

Microscale, Laser Peen Forming, Deformation

ABSTRACT

Microscale laser peen-forming (μLPF) is an innovative process in which compressive residual stress is induced into the treated surface to improve fatigue life of the micro scale metallic parts and meanwhile shape the parts with a controlled bending deformation. In this work, dynamic deformation in μLPF of single crystal aluminum is investigated. A finite element model based on meso scale crystal plasticity integrated with consideration of dynamic effects is implementated to simulate the shock wave propagation in aluminum single crystal and to predict the deformation, lattice rotation and the induced surface residual stress distributions in μLPF. The crystal elastic moduli are pressure dependent to capture the large volume strains properly and to enable evolution of shocks from steep pressure gradient. Experimentally, local plastic deformation as well as residual stress distributions on both top and bottom surfaces measured by X-ray micro-diffraction, is compared with the results obtained from FEM simulation.

INTRODUCTION

In laser shock processing, shock-compression process is quite different from those events under normal loading. When material bodies are subjected to rapid impulsive loading, whose time of load application is short compared to the time of the body to respond inertially, the material's mechanical response is fluid-like (Asay et al. 1992). In isotropic solids, the Mie-Grüneisen equation of state is applied to describe the fluidlike hydrodynamic behavior under such a high pressure in laser shock processes (Fan et al. 2005). Most metallic single crystal exhibit cubic symmetry that leads to anisotropy in their physical properties such as the elastic constants and wave propagation velocity. This anisotropy leads to a more complex shock-induced dynamic deformation in μLPF of single crystal.

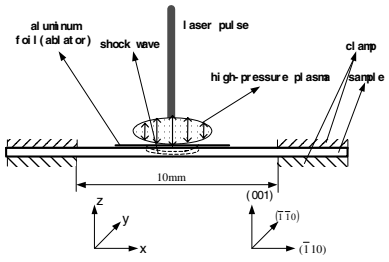

FIGURE 1. SAMPLE GEOMETRY AND LASER PEENING FORMING CONDITIONS.

In this work, the dynamical response and anisotropy in micro-scale laser peen forming of aluminum single crystals have been numerically and experimentally investigated. A finite element model based on meso scale crystal plasticity (Asaro 1983) integrated with consideration of dynamic effects and the pressure dependence of the elastic moduli is implementated to simulate the shock wave propagation in aluminum single crystals and to predict the deformation, lattice rotation and the induced surface residual stress distributions in μLPF. Experimentally, synchrotron X-ray mircodiffraction is used to measure the surface residual stress caused by high-strain rate line shock compression in the [110] direction on (001) surface (Fig. 1). In addition, the bending curvature is measured by profilometery. The experimental results are compared with the numerical results and provide useful insight into the dynamic shock peen-forming process of single crystal.

DYNAMIC MODELING OF μLPF

Basic Assumptions of the Modeling

The goal of this work is to explore the dynamic anisotropic effects in μLPF under high pressure loading. This requires extending the crystal plasticity model to regimes characteristic of laser induced shocks. The pressures are as high as 10 GPa and the strain rates can exceed 10^6 s^{-1}. Therefore the modeling is based on the below assumptions:

1. Although the pressures and strain rates are outside of the range where crystal plasticity models have been validated, existing models are employed to perform an approxiamate analysis.
2. Glide is assumed to be the only plastic deformation mechanism. The volume change caused by hydrostatic compression does not influence plastic deformation. The change of internal energy caused by hydrostatic compression is neglected in this work.
3. Single crystal aluminum under shock loading follows crystalline plasticity and isotropic elasticity.
4. Deformation caused by laser induced line pressure loading in the [110] direction on the (001) plane in the μLPF is assumed to follow plane strain condition to form two-dimensional deformation (Kysar and Briant 2002).

Pressure Dependent Moduli

When high pressure is applied to metals, the elastic properties of metals depend on the applied pressure. It is important to include the pressure dependence of the moduli. Without pressure dependent moduli, shocks can not form. Therefore, a constitutive model is required to account for the effect. The model significant departs from prior work is to consider both dynamic effects and anisotropy in micro scale LPF as well as incorporate the pressure dependence of the elastic properties.

It is common to assume that the elastic response of a single crystal under high pressure is isotropic. Thus, the well known Steinberg-Guinan model (Steinberg et al. 1980) can be applied for taking account of pressure dependent of the elastic moduli:

$$G = G_0[1 + A_0 \frac{P}{\eta^{1/3}}] \qquad (1)$$

where η is compression, defined as $\eta = \frac{\rho}{\rho_0}$, the constants G_0 and A_0 are determined from the measured values of shear modulus and its first derivative at ambient conditions, P is pressure in GPa. Because of the assumed elastically isotropy, the pressure dependent elastic moduli are determined by:

$$C11 = \frac{2G(1-\nu)}{1-2\nu},\ C12 = \frac{2G\nu}{1-2\nu},\ C44 = G \qquad (2)$$

where ν is Poisson ratio. The laser induced shock loading during laser shock peenforming is a weak shock loading, and under a weak shock loading, the Poisson ratio is almost pressure independent (Shehadeh et al. 2005).

The implementation of the above nonlinear elastic model in the finite element framework required the adjustment of the stiffness matrix at every time step. At each step, the pressure P requires adjusting. In the continuum mechanics community, pressure is usually defined as $P = -(\sigma_{11} + \sigma_{22} + \sigma_{33})/3$ □ and in the shock wave community, the pressure is usually given by $P = -\sigma_{33}$ (Shehadeh et al. 2005). It can be found that these two definitions coincide only in the case of uniaxial strain of isotropic linear elastic material with Poisson's ratio of 0.5. In this paper, the definition of $P = -\sigma_{33}$ is used.

Hardening of Rate Dependent Crystalline Materials

In the finite element analysis, the stresses, strains and lattice rotation were solved incrementally by ABAQUS using a finite strain kinematic structure described by Huang (1991). A power-law rate-dependent relationship described by Peirce et al. (1983) was used:

$$\dot{\gamma}_k = \dot{\gamma}_0 \operatorname{sgn}\left(\tau^k\right)\left\{\left|\frac{\tau^k}{\tau_0^k}\right|\right\}^{1/m} \quad (3)$$

where is $\dot{\gamma}_0$ the reference strain rate, τ^k is the applied resolved shear stress, m is the rate sensitivity exponent, and τ_0^k is related to critical resolved shear stress of the k[th]-slip system, as given by Peirce et al. (1983). When $m = 0$, it means that the material is rate independent. The condition $m = 1$ implies that shear stress τ^k is proportional to sliding rate $\dot{\gamma}_k$, a relation identical to a Newtonian fluid. Under shock loading, mechanical response of single crystal aluminum is neither static nor ideally like Newtonian fluid, so an intermediate value 0.1 of m is applied in this paper. In addition, based on Asaro's hardening theory of single crystal (Asaro 1983), the critical shear stress τ_0^k of the Schmid law is determined by the current dislocation density and substructure, and represents variation of hardness of material due to work hardening. Since work hardening of slip system depends on shear deformation of slip systems, variation of τ_0 may be estimated by

$$\{\Delta\tau_0\} = [h]\{|\Delta\gamma|\} \quad (4)$$

where h expresses hardening rate. h_i^k is hardening rate against increment of shear deformation $\Delta\gamma_i$ on each slip system. When k equals to i, h_i^k represents hardening by glide on its own slip system. When k is not the same as i, h_i^k represents hardening by glide on other slip systems. The former is called the self hardening, and the latter is called the latent hardening. The ratio denoted by q between latent hardening rate and self hardening rate can be evaluated by the following equation (Asaro 1983):

$$h_i^k = qh + (1-q)h\delta_{ij} \quad (5)$$

and q = 1.4 is best to match simulation with experimental results. Where h is given by

$$h = h_0 \operatorname{sech}^2\left(\frac{h_0\gamma}{\tau_{\max}^k - \tau_0^k}\right) \quad (6)$$

$$\gamma = \sum_i |\Delta\gamma_i| \quad (7)$$

where $\tau_{\max}^k$ is the maximum value of yield shear stress and h_0 is a material constant. In this paper, $\tau_0^k = 42.0MPa$ (Shiina et al. 1998), $h_0 = 8.9\tau_0$ and $\tau_{\max}^k = 1.8\tau_0$ are used (Asaro 1983).

Simulation Conditions

A user-material subroutine (UMAT) for single crystal plasticity based on theory in Asaro (1983) and written by Huang (1991) is incorporated into the finite element analysis using the general purpose finite element program ABAQUS/Standard.

Since the surface deformation and lattice rotation under laser peen forming indicate that an approximate two-dimensional deformation state exists, we will assume that the induced deformation state is strictly two-dimensional. Therefore a two-dimensional dynamic simulation is performed. The boundary conditions of the plane strain model are as follows. At the top surface, surface traction equals the applied shock pressure, at the bottom surface is traction free and the clamped ends are fixed. Because the deformation caused by line loading in the [110] direction on the (001) plane is symmetric, only half of the single crystal aluminum strip is calculated, and the displacement in x direction of the central surface (x = 0 mm) is fixed and equals zero. To eliminate "volume-locking" which occurs in plastic deformation simulation, 4-node linear elements with reduced integration and hourglass stiffness control are used. The element type is CPE4RH. The elements are biased laterally and vertically away from the load center, and fine elements are used in the area around the shock load center. The finest grid is around 0.5 μm, and the overall thickness and length of the meshed region was 150 μm and 10 mm, respectively.

EXPERIMENTS

A frequency tripled Q-switched Nd:YAG laser ($\lambda = 355\ nm$) in TEM00 mode was used in micro-scale LPF. Pulse duration is 50 ns and laser beam diameter is 12 μm. If a line loading is

applied parallel to a <110> direction in a FCC crystal, certain slip systems act cooperatively which enable plane deformation conditions to be achieved (Rice 1987). Therefore, a line of μLPF shocks parallel to a <110> direction was created on the sample surface with a 25 μm spacing because this spacing results in approximate 2-D deformation. Pulse energies, 202 and 280 μJ, corresponding to laser intensities of 3.57 and 4.95GW/cm^2, respectively, were applied. A thin layer of high vacuum grease (about 10 microns thick) was spread evenly on the sample surface to isolate the thermal effect from the coating, and a 16 μm thick polycrystalline aluminum foil, chosen for its relatively low threshold of vaporization, was tightly pressed onto the grease. The sample was placed in a shallow container filled with distilled water around 1 mm above the sample's top surface to confine the produced plasma. The induced deformation is due to shock pressure and not due to thermal effects since the aluminum foil coating served as an ablator to protect the workpiece from thermal effect. The samples of single crystal aluminum with 150 μm thickness have normal orientation of (001) as shown in Fig. 1. The samples were cut to the dimension of 20mm×3mm by using a wire electrical discharge machining (EDM) and mounted to holders as shown in Fig. 1 carefully to make them as flat as possible. The sample surface on both sides was polished mechanically first to remove the heat effected layer by EDM and then electro-polished to remove the stressed layer caused by mechanical polishing. Before the shocking process, the pre-bending is measured by using a Mitutoyo SJ-201P profilometer and the samples only with a pre-bending less than 6 μm were chosen to minimize pre-bending effects.

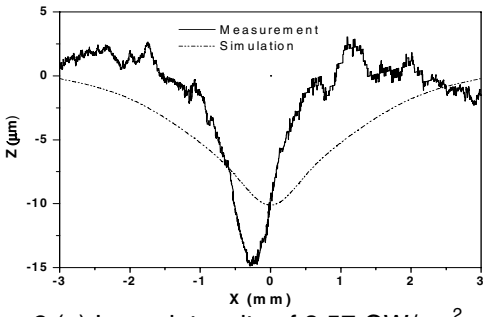

2 (a) Laser intensity of 3.57 GW/cm^2

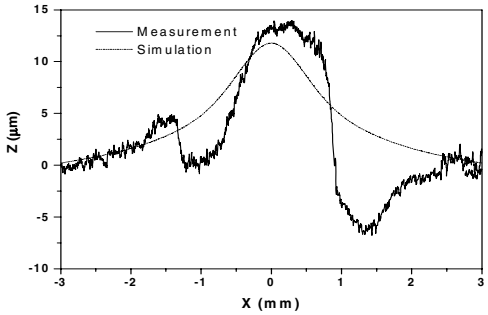

2 (b) Laser intensity of 4.95GW/cm^2

FIGURE 2. BENDING CURVATURE COMPARISON BETWEEN SIMULATION AND MEASUREMENT.

After laser shock peen-forming, the deformation was characterized by curvature change, residual stress distribution and lattice rotation. It is obvious that the first two characterizations are necessary so that we can study the capability of micro-scale curvature adjustment by μLPF and its potential to improve fatigue life. The curvature change is characterized by using profilometer measurement. Residual stresses were estimated from X-ray micro-diffraction profiles, which were collected from Beamline X20A (synchrotron radiation sources) at Brookhaven National Laboratory. X-ray of X20A which can be focused by a tapered glass capillary to spot sizes as small as 3 microns. It should be noted that the measured residual stress is an approximate average value through the X-ray penetrated depth. Complete details of X-ray micro-diffraction experiment and the corresponding evaluation method of sub-profile analysis can be found in prior work (Fan et al. 2005).

RESULTS AND DISCUSSIONS

Bending Curvature Validation

The comparison of bending curvatures caused by μLPF between the measured and the numerically predicted value is shown in Fig. 2. Fig. 2(a) shows the case of low laser intensity of 3.57 GW/cm^2. Experimentally, after laser shock peen forming the strip was bent downward, and the net bending height was about -15 microns. Numerically, the bending height was around -11 microns and roughly matched the experimental results. In Fig. 2(b) for the case of high laser intensity of 4.95 GW/cm^2, the strip was bent upward by μLPF, and the bending height was about 13 microns. In this case, the numerically predicted deformation and the experimental are

in good agreement. Prior work (Fan et al. 2005) showed that 100μm poly copper with 4.95GW/cm^2 laser intensity was bent upward and compressive residual stress was induced into both the top and bottom surfaces; however, with low energy of 3.57GW/cm^2 laser intensity the poly copper sample was bent downward, and compressive residual stress was imparted into the bottom surface while tensile residual stress was induced into the top surface. Wang, et al. (2005) explained why laser energy levels have effects on bending mechanisms in μLPF of poly copper. For single crystal aluminum, it can be seen from Fig. 2 that those experimental and numerical results are consistent with the cases of poly copper samples and the detail explanation can refer to the previous work (Wang et al. 2005).

Residual Stress Distribution Validation

Fig. 3 shows the comparison of surface residual stress distributions between the measured and the calculated values. To spatially resolve the residual stress induced by μLPF, measurements were made on both top and bottom surfaces across the shocked line. The spacing between adjacent measurement points is 10 μm and the corresponding X-ray diffraction profile at each position is recorded and repeated for each scan line. The measured residual stress can be considered to be average residual stress within the X-ray penetrated depth in the region sampled by X-ray diffraction. Although the laser spot size is only 12 μm, the high shock pressure in μLPF can generate significant compressive residual stresses over a much larger region. In Fig. 3 (a), the comparison of surface residual stress distributions for the case of low laser intensity of 3.57GW/cm^2 is given. From Fig. 3(a), the measured region on the top surface with tensile residual stress is about 200 μm wide, and the induced peak tensile residual stress is about 80 MPa. On the bottom surface, the induced peak compressive residual stress is -75 MPa. Similarly, the simulation also predicts that a tensile residual stress is induced on the top surface while compressive residual stress is imparted into the bottom surface. From the comparison, the calculated bottom surface residual stress distribution matches the results from the measurement pretty well, but the calculated top surface residual stress profile is narrower than the measured residual stress profile and the calculated peak residual stress (75MPa) is smaller than the measured. This is because hydrostatic compression on the top surface in this simulation is neglected, and since hydrostatic compression gvies the single crystal aluminum a fluid-like behavior, the result is a larger plastic deformation zone, and in turn, a wider induced residual stress region. Fig. 3(b) gives the comparison of surface residual stress distributions for the case of high laser intensity of 4.95 GW/cm^2. The comparison also shows that numerically and experimentally, compressive residual stress was induced into both top and bottom surfaces of the sample and the simulated residual stress distributions are in good agreement with the experimental results. From Fig. 3, it is found that under different energy levels, the induced surface residual stress distributions are different. A prior work (Wang, et al., 2005) has explained that the induced surface residual stresses are closely related to bending mechanisms, and in turn, to laser energy levels.

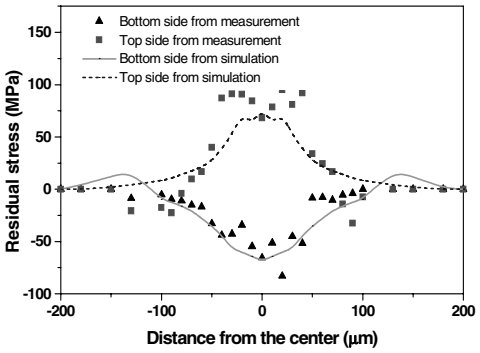

(a) Laser intensity of 3.57 GW/cm2

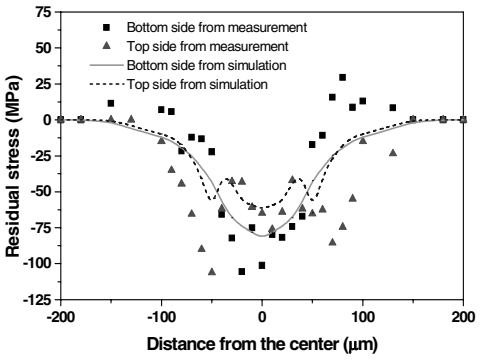

(b) Laser intensity of 4.95GW/cm2

FIGURE 3. COMPARION OF SURFACE RESIDUAL STRESS DISTRIBUTIONS BETWEEN THE MEASURED AND THE CALCULATED.

Fig. 4 shows the comparison of the simulated residual stress distribution in the single crystal

aluminum sample between quasi-static FEM simulation of μLPF (Wang et al. 2006) and dynamic FEM simulation. The applied laser intensity is 3.57GW/cm^2. From Fig. 4(a), the residual stress was mainly induced in the middle layer of the sample, and the induced surface residual stress is very small. Both the residual stress distribution pattern and magnitude are quite different from the experimental results. In addition, the quasi-static simulation shows that there is almost no local plastic deformation in the shocked area. These results from quasi-static simulation are quite different from experimental observations and measurement, and in the previous work (Chen et al. 2004; Wang et al. 2005), the quasi-static simulation was only used as a qualitative method to analyze μLSP and μLPF. From Fig 4(b), the numerical results from dynamic simulation are well matched by the experimental results based on the comparison in Fig. 3 (a). Therefore, it is very necessary to consider the dynamic effects in micro scale laser peen forming.

Based on the above comparisons of bending curvatures and surface residual stress distributions between the measurements and the s, it is seen that the proposed dynamic model gives reasonable results..

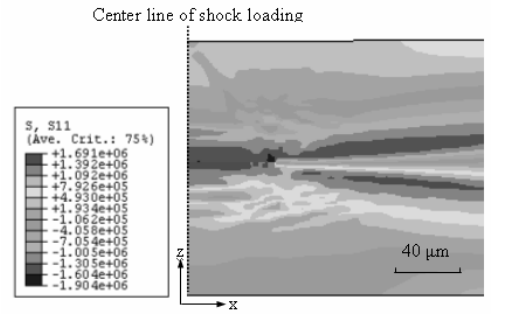

(a) Quasi-static simulation

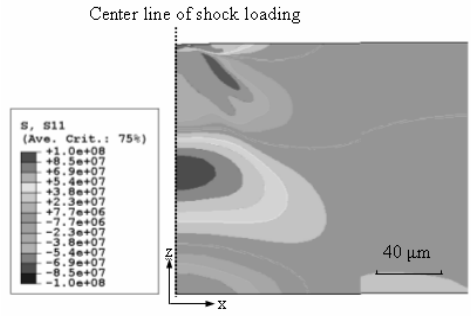

(b) Dynamic simulation

FIGURE 4. COMPARISON OF THE SIMULATED RESIDUAL STRESS DISTRIBUTION BETWEEN QUASI-STATIC FEM SIMULATION OF μLPF (WANG ET AL. 2006) AND DYNAMIC FEM SIMULATION.

Effects on Anisotropic Deformation

For a face-centered cubic crystal of aluminum, there are a total of twelve plastic slip systems {111}<110>. If a line loading is applied parallel to a <110> direction in a FCC crystal, certain slip systems act cooperatively which enable plane deformation conditions to be achieved (Rice 1987). As discussed in detail by Kysar and Briant (2002), the $(\bar{1}11)[011]$ and $(\bar{1}11)[\bar{1}01]$ slip systems can act cooperatively and in equal amounts to form an effective in-plane slip system which induces plastic deformation in the $[\bar{1}12]$ direction which lies within the (110) plane. This effective in-plane slip system is denoted as slip system I in Fig. 5. Likewise, the $(\bar{1}11)[101]$ and $(\bar{1}11)[0\bar{1}1]$ slip systems can act cooperatively and in equal amounts to form an effective slip system which induces plastic deformation in the $[1\bar{1}2]$ direction which lies within the (110) plane. This effective in plane slip system is denoted as slip system II in Fig. 5. Similarly, the $(111)[\bar{1}10]$ and $(11\bar{1})[\bar{1}10]$ slip systems act cooperatively and in equal amounts to form an effective slip system which induces plastic deformation in the $[\bar{1}10]$ direction which lies within the (110) plane. This effective in plane slip system is denoted as slip system III in Fig. 5. Thus, a loading which can be approximated as a distributed line loading along [110] generates a predominately plane deformation state in (110) plane. Rice (1987) showed that the remaining slip systems do not contribute significantly to sustained in-plane plastic deformation.

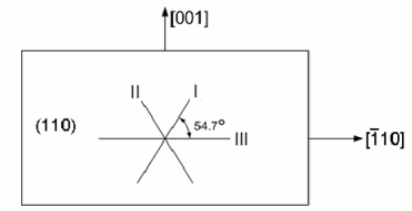

FIGURE 5. THREE PAIRS OF EFFECTIVE SLIP SYSTEMS UNDER PLANE STRAIN CONDITIONS IN SINGLE CRYSTAL ALUMINUM.

Fig. 6 shows the simulated shear strain fields for the three slip systems for the case of high laser intensity of 4.95GW/cm^2. Based on the above analysis, the resulting shear strain field for the slip system I should be mirror symmetric

to that of the slip system II. The numerical results only show half of the single crystal aluminum strip. However to clarify the presentation of results, the fields are shown as if for the entire specimen in Fig. 6(a). The shear strain in slip system III is symmetric to the axis Z and the calculated shear strain for slip system III shown in Fig. 6(b) is much smaller in magnitude than those for the slip systems I and II because Schmid's factor is zero for slip system III. Fig. 7 shows the simulated shear strain field on slip system I by quasi-static FEM simulation of μLPF under the same conditions (Wang, et al., 2006). Comparing Fig. 7 with Fig. 6(a), it is found that in dynamic simulation the shear slip mainly took place under the 54.7° slip line (shown in Fig. 5), and the region is much smaller while the magnitude of shear strain is much larger. In quasi static simulation, a long loading time (1 second) and a low peak pressure are applied to obtain a similar plastic deformation. A lower pressure loading with a longer loading time makes the plastically deformed region bigger but the deformed region is smaller. In the dynamic case, the loading duration is very short, and loading radius is only 12 microns, so the loading in dynamic case is more like point loading. That is why the shear strain patterns in Fig. 7 and Fig. 6(a) are different.

(a) Slip system I

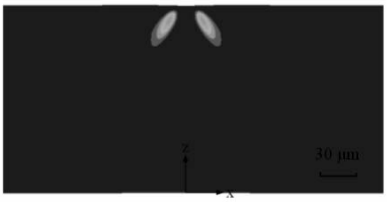

(b) Slip system III

FIGURE 6. SHEAR STRAIN FIELDS ON ACTIVE SLIP SYSTEMS BY DYNAMIC SIMULATION OF μLPF WITH HIGH LASER INTENSITY OF 4.95GW/cm^2.

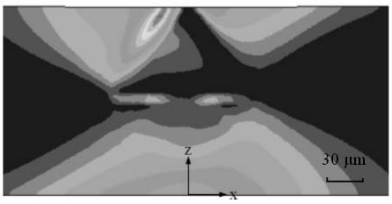

FIGURE 7. SIMULATED SHEAR STRAIIN FIELDS ON SLIP SYSTEM I BY QUASI-STATIC FEM SIMULATION OF μLPF (WANG ET AL. 2006).

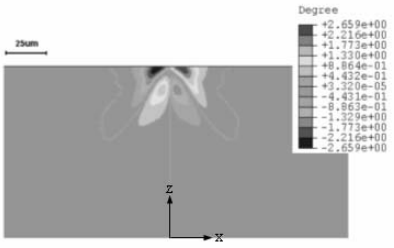

(a) Laser intensity of 3.57GW/cm^2

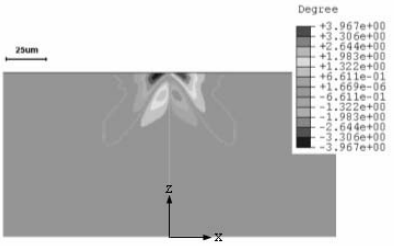

(b) Laser intensity of 4.95 GW/cm^2

FIGURE 8. COMPARISON OF DYNAMIC FEM SIMULATION OF μLPF BETWEEN DIFFERENT LASER INTENSITY LEVELS.

Effects on Lattice Rotations

The calculated lattice rotation contours in the cross sections corresponding to the two different energy levels are shown in Fig. 8. In the lattice rotation contour maps, the red region corresponds to counter-clockwise rotation about the y-axis which is positive and the blue region corresponds to clockwise rotation which is negative. In addition, from the lattice rotation contour maps, the lattice rotation is anti-symmetric about the shock line. From both Fig. 8 (a) and (b), the lattice rotation distributions are similar except that the rotation angle in the high laser intensity case is bigger. In addition, both Figs. 8 (a) and (b) show that in the simulated lattice rotation fields the direction of lattice rotation is changed across a line which is about 45° from the top surface, however more study is necessary to understand the details of the mechanisms which lead to this behavior.

CONCLUSIONS

In this work, micro scale laser peen forming has been experimentally and numerically investigated. Numerically, a FEM model based on meso scale crystal plasticity integrated with consideration of dynamic effects is implementated to simulate dynamic deformaion in aluminum single crystal and to predict the lattice rotation and the induced surface residual stress distributions. Experimentally, bending curvature and surface residual stress distributions have been measured. Both simulation and measurement show that when the single crystal aluminum strip was bent downward with low laser intensity, compressive residual stress was imparted into the bottom surface while the tensile residual stress was induced to the top surface, and that when the single crystal aluminum strip was bent upward with high laser intensity, compressive residual stress was induced into both top and bottom surfaces. The analysis of lattice rotation and anisotropic deformation also shows that the proposed model is capable to well predict a μLPF process.

REFERENCES

Asaro, R.J. (1983). "Micromechanics of Crystals and Polycrystals." *Adv. Appl. Mech*., Vol. 23, pp. 1-15.

Assay, J.R. and M. Shahipoor (1992). *High-pressure Shock Compression of Solids*. New York, Springer-Verlag, pp. 8-12.

Chen, H., J.W. Kysar, and Y.L. Yao (2004). "Characterization of Plastic Deformation Induced by Micro Scale Laser Shock Peening." *Journal of Applied Mechanics*, Vol. 71, pp. 713-723.

Fan, Y. et al. (2005). "Wave-Solid Interactions in Laser Shock Induced Deformation Processes." *Journal of Applied Physics*, Vol. 98, pp. 104904[1-11].

Huang, Y. (1991). "A User-Material Subroutine Incorporating Single Crystal Plasticity." ABAQUS Finite Element Program, Mech. Report 178., Division of Applied Sciences, Harvard University, Cambridge, MA.

Kysar, J.W. and C.L. Briant (2002). "Crack Tip Deformation Fields in Ductile Single Crystals." *Acta Materialia*, Vol. 50, pp. 2367-2380.

Peirce, D., R. Asaro, and A. Needleman (1983). "Material Rate Dependence and Localised Deformation in Crystalline Solids." *Acta Metall. Mater.*, Vol. 31, pp. 1951-1976.

Rice, J.R. (1987). "Tensile Crack Tip Fields in Elastic-Ideally Plastic Crystals." *Mechanics of Materials*, Vol. 6, pp. 317-335.

Shehadeh, M.A. et al. (2005). "Modelling the Dynamic Deformation and Patterning in FCC Single Crystal at High Strain Rates: Dislocation Dynamics Plasticity Analysis." *Philosophical Magazine*, Vol. 85, pp. 1667-1685.

Steinberg, D.J. et al. (1980). "A Constitutive Model for Metals Applicable at High Strain Rate." *J. Appl. Phys.*, Vol. 51, pp. 1498-1504.

Wang, Y., Y. Fan, S. Vukelic, and Y.L. Yao (2005). "Energy Level Effects on Deformation Mechanism in Micro-scale Laser Peen Forming." Submitted to *J. of Manufacturing Processes*.

Wang, Y., Y. Fan, S. Vukelic, J.W. Kysar, and Y.L. Yao (2006). "Micro-scale Laser Peen Forming of a Single Crystal." In progress.